https://doi.org/10.48047/AFJBS.6.15.2024.144-153

AFJBS

African Journal of Biological Sciences

Journal homepage: http://www.afjbs.com

Research Paper Open Access

Development and characterization of nanocomposite with nanoparticles of neem leaf extract and silver - zinc

[1]Ekta Sharma, [2]Pradyuman Kumar

[1,2]Department of Food Engineering and Technology, Sant Longowal Institute of Engineering and Technology, Longowal 148106 (Punjab) India

[1] sharmaekta2508@gmail.com, [2]pradyuman2002@hotmail.com

Volume 6, Issue 15, Sep 2024

Received: 15 July 2024

Accepted: 25 Aug 2024

Published: 03 Sep 2024

doi: 10.48047/AFJBS.6.15.2024.144-153

Abstract - In the present study, composite film was prepared by blending neem leaf extract with a selected concentration of nanocomposite silver and zinc and its characterization. Silver nitrate and zinc oxide were used as precursors for the nanocomposite of Ag-Zn synthesis. Neem leaves consist of various phytochemicals, polyphenols, and quercetin which help in the reduction of the chemical salt into the nanoparticles and act as the capping agent. Our result showed that the nanocomposite of Ag-Zn nanoparticles was grey. UV spectroscopy shows the maximum peak at 423nm. The average crystallite size reported for nanocomposite Ag–Zn Np was 35.38 nm. The antioxidant activity was enhanced up to 88.15%. Homogeneous growths on the surface were shown in SEM images of Ag-Zn Np. Also by using chitosan and guar gum composite films modified with Ag-Zn nanoparticles for packaging. The distribution of Ag-Zn nanoparticles in films was uniform. Ag-Zn NPs loaded films were constructed by a simple solvent casting method and were found to be polished smooth and flexible. Transparency, tensile strength, and opacity increased. WVTR and WVP value was lowered. Tensile strength increases due to the presence of microfibers and polyphenols in the neem leaf extract and elongation at break decreases as the increase in the compatibilization between the polymers reduces the flexibility of film.

Keywords: Nanocomposite, Neem leaf extract, Silver nitrate and zinc oxide, WVTR

1. Introduction

Azadirachta indica is generally called a Neem. An evergreen tree of the Meliaceae family, belonging to India, traditionally used for thousands of years in medicine and Ayurveda [1]. Nanotechnology has many positive effects on the food sector, including the costs involved, environmental hazards, disease finding to stop losses, and management of farm practices [2]. ZnO nanoparticles (NPs) have diverse shapes (rod-like, star-like, and isometric) and a broad size distribution range of 30–150 nm. The ZnO particles are generally present as bunches. In addition, spherical particles with a size between 200 nm and 1 µm were present (Dash e. silver nanoparticles (Ag NPs) are more efficient in fighting pathogenic microbes such as viruses, bacteria, yeast, and fungi [3]. Nanocomposite's small size and large surface area to volume ratio give them better physical, biological, and chemical properties as related to their large-scale counterparts. AgNPs and Zn-NPs have been verified to have effective antimicrobial activity at very low concentrations even to resistant strains of microbes. This is because they dismiss many biological pathways in a cell and it would require the microorganism to go through many coexisting transmutations to develop resistance against them [4]. Composite films are thin layers of edible material that are molded as a protective coating or layer on foods and can be consumed together with food products. They aid as a wall between oxygen, moisture, and the surrounding environment. They can additionally be utilized to detach different compartments of the same food. By limiting the exchanges between foods and their surrounding atmosphere, they can reduce water loss, oxidation reaction rates, and respiration rates, ultimately extending the shelf life of the food product [5].

2. Materials and Methods

Chemicals of analytical grade were sourced from Loba Chemical Pvt Ltd. Various chemicals such as sodium Carbonate, Aluminium chloride, DPPH, folin ciocaleteau reagent, sodium hydroxide (NaOH), pH buffers, zinc oxide, silver nitrate, guar gum, and chitosan were used for the experiment.

S. No	Films	Extract composition (g)	Nanoparticle's composition (g)
1	CS/GG	0	0
2	CS/GG/NLEx	2	0
3	CS/GG/Ag-Zn NPs	0	2
4	CS/GG/25NLEx/75 Ag-Zn NPs	0.5	1.5
5	CS/GG/50NLEx/50 Ag-Zn NPs	1	1
6	CS/GG/75NLEx/25 Ag-Zn NPs	1.5	0.5

2.1 Synthesis of Ag-Zn nanocomposite

A two-step preparation of Ag–Zn nanocomposite was performed. First, a 0.9 M zinc sulphate solution was made in 20 ml double distilled water, and 5 ml neem extract was also added dropwise. NaOH solution was gradually added to maintain the pH of the solution at 12. When NaOH was added, the color of the solution showed an alteration from watery to milky. Now in the above solution, 0.1 M silver nitrate solution was added. The solution turned a dark reddish hue. The solution is stirred on a magnetic stirrer at 60°C for 30 minutes. The resulting precipitates are filtered, concurrently washed with double-distilled water and methanol, and dried for further assessment [6].

2.2 Characterization of synthesized Ag-Zn nanocomposite

Absorbance of Ag-Zn nanoparticles was analyzed using UV-spectroscopy wavelength ranges from 200-500 nm. The FT-IR spectrum of the nanoparticles was recorded at room temperature in transmittance mode across the 4000-400 cm^{-1} region. The X-ray diffraction (XRD) patterns were used to analyze the crystal domain sizes of the nanoparticles using the Scherrer formula. The surface morphology of the Ag-Zn nanoparticles was observed using scanning electron microscopy (SEM) (JEOL, JSM 6300 SEM, Japan). The fractured films were mounted on aluminum stubs using double-sided carbon adhesive tape and coated with a thin layer of gold. All samples were examined using an accelerating voltage of 7 kV. The antioxidant activity 2,2-Diphenyl-1-picrylhydrazyl (DPPH) of the Ag-Zn nanocomposite was studied wavelength of 515 nm.

2.3 Preparation and studies of the nanocomposite film modified with Ag-Zn nanoparticles

Film was prepared using the casting method according to Yadav et al., (2020) with some minor modifications. Chitosan nanocomposites reinforced with guar gum were prepared by solution casting. Chitosan was made by dissolving 2.5 g of chitosan flakes into 1% (v/v) glacial acetic in 250ml of distilled water and mechanically stirred for 15 minutes at 35°C. The film-forming solution was formed by combining 2 g of Guar gum (GG) granules with 150 mL of distilled water at 60ºC for 5 minutes while vigorously magnetic stirring. Subsequently, the solutions obtained above were combined in a ratio of 3:7, and 150 ml was used for preparing the film 1% (v/v) glycerol was added as a plasticizer in the above mixture to obtain CS/GG film it was easy to add just the prepared solution in the Teflon-coated mold. Neem leaf extract and Ag-Zn NPs were varied in composite film production as per Table 1. Then the solution was transferred to a tray drier in Teflon-coated mold and dried at 45°C until the solvent was completely evaporated, and a self-standing film was attained.

Table 1 Formulation for Preparation of Composite Film

Analysis

The moisture content of the film was measured using the AOAC method. For determining sheet thickness, a handheld micrometer (Alton M820-25, China) with a sensitivity of 0.01 mm was used. Film transparency was measured with a UV-visible spectrophotometer at 600 nm. The mechanical properties, including tensile strength (TS) and elongation at break (E%), of the films were measured using a texture analyzer (Stable Micro Systems, Surrey, UK), following ASTM 828-97 (ASTM, 2002) standards. Film solubility tests were determined gravimetrically.

The WVP of the film samples was calculated following the ASTM E96 (1995) specification with slight modifications. The total phenol content of the films was estimated using the Folin-Ciocalteu method. The antioxidant activity 2,2-Diphenyl-1-picrylhydrazyl (DPPH) of the films was projected to wavelength around 515 nm. Color measurements of the samples in terms of L*, a*, and b* values were conducted using a Hunter Colorimeter Model D25 Optical Sensor. The FT-IR spectra of the film samples were obtained at room temperature in transmittance mode across the 4000-400 cm^{-1} region. XRD patterns of the films were measured using a diffractometer with Cu Kα radiation operating at 30 kV and 15 mA. The surface and crosssectional morphologies of chitosan-based films were examined using an SEM. The thermal stability of the films was assessed using a thermogravimetric analyzer (TGA/DSC 1 star system, Mettler Toledo, Switzerland).

3. Results and Discussion

3.1 Characterization of Ag-Zn nanocomposite

3.1.1 Visual observation

In the two-step preparation of the Ag-Zn nanocomposite, adding zinc oxide to 20 ml of double-distilled water resulted in no observable changes. However, when NaOH solution was added dropwise, the color of the solution transformed from clear to milky, as depicted in Figure 1. Upon addition of silver nitrate solution to this mixture, the solution turned a dark reddish color.

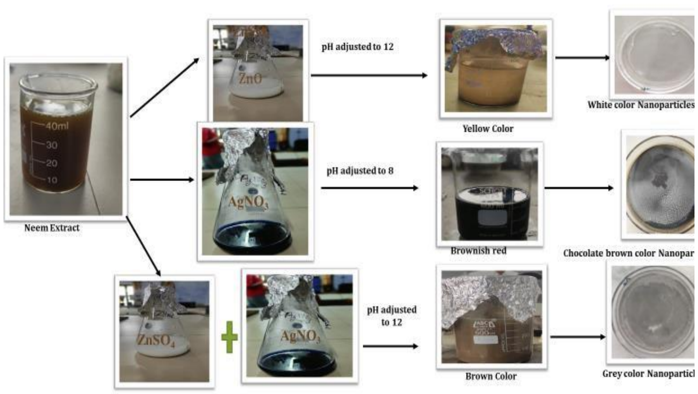

Figure 1 Color changes observed in ZnO, $AgNO_3$and Ag-Zn Nanocomposites

3.1.2 UV–Visible spectroscopy

In the case of nanocomposite $AgNO_3$ ZnO nanoparticles at 423nm peak was observed which confirms the interaction of zinc, silver, and neem extract Figure 2. The wide bandgap of bare ZnO makes its use intolerable. Therefore, coupling it with Ag had the result of effectively reducing the energy bandgap. Hence, as demonstrated by Slathia et al. (2021), contributes to an increase in the rate of organic contaminants' erosion under visible light (7).

3.1.3 X-ray diffraction pattern

Ag-Zn NP supported the hexagonal wurtzite structure of ZnO NPs at the peaks located at 31.81, 34.45, 36.28, 47.58, 56.611, 66.36, 67.91, 69.09, and 72.54, which are enumerated as (100), (002), (101), (102), (110), (103), (200), (112), (201), and (004) planes, respectively. The peak intensity observed at the (101) plane in both cases indicated that the ZnO nanoparticles exhibited a strong preferred orientation along this plane. The distinct patterns of Ag and ZnO confirmed the presence of a metallic Ag phase on the surface of ZnO, supported by the larger ionic radius of Ag+ (126 pm) compared to Zn2+ (74 pm). This observation validates the formation of a crystalline nanocomposite, as reported by [8]. Using Debye Scherrer's method, the mean crystallite size of the Ag-Zn nanocomposites is determined. The average crystallite size reported for nanocomposite Ag–Zn NP was 35.38 nm. Figure 3 shows XRD data of the sample as coded in the image (A) ZnO NpS (B) Ag NO_3 NpS and (C) Ag-Zn NpS.

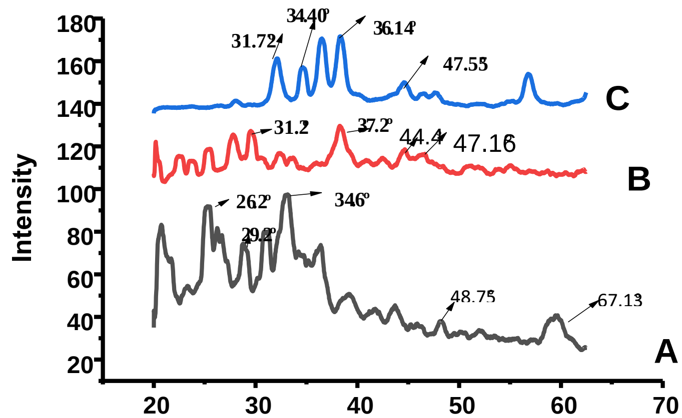

Figure 2 UV Spectroscopy data of sample as coded in the image (A) ZnO NpS and (B) Ag NO_3 NpS and (C) Ag-Zn NpS

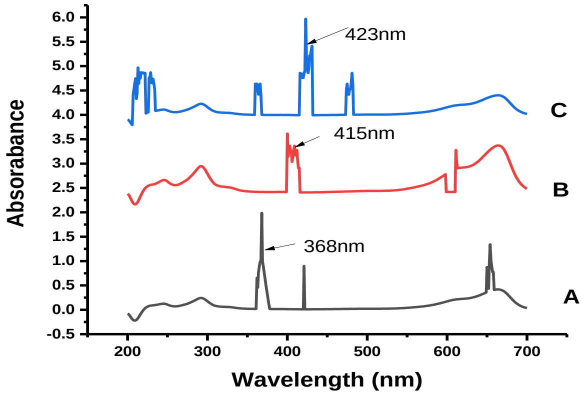

Figure 3 XRD data of sample as coded in the image (A) ZnO NpS and (B) Ag NO_3 NpS and (C) Ag-Zn NpS

3.1.4 Antioxidant Activity

The antioxidant activity of ZnO NP is 58.78±0.09, $AgNO_3$ NP is 62.55±0.04 and Ag-Zn NPs is 88.15±0.06. With the rise in the quantity of Ag-Zn NCs, the antioxidant activity is enhanced by 88.15±0.06[a]. The scavenging potency of samples was observed by [9] at 91.42% at the highest amount of 100 µg/ml for Ag-Zn NCs. The acquired Ag-Zn NCs retained an increase in their scavenging efficacy. Ag incorporated into ZnO NPs significantly enhances their oxidation activities. The nanocomposite's synergistic impact may be to blame for this. In terms of removing DPPH free radicals, this indicates that the synthesized Ag-Zn NCs have higher antioxidant activity. The inherent scavenging potency of ZnO and AgNP has been extensively studied. We therefore believe that the collective effect of ZnO and Ag NPs has demonstrated significant scavenging potency [10].

4.1.5 Fourier transform infrared (FT-IR)

A broad range of many phytochemicals in the Neem leaf extract has reducing properties that result in the fast bioreduction of zinc ions into nano-scaled ZnO particles. Some phytochemicals such as flavones, organic acids, and quinones are involved in the bioconversion process. Through the process of incubating benzoquinones in neem, quinone activation reduced the mean particle size of nanoparticles. A comparison of the FT-IR analyses of ZnO-NPs and hybrid nanoparticles revealed the extract of Azadirachta indica to have reducing and capping abilities. (Figure 4).

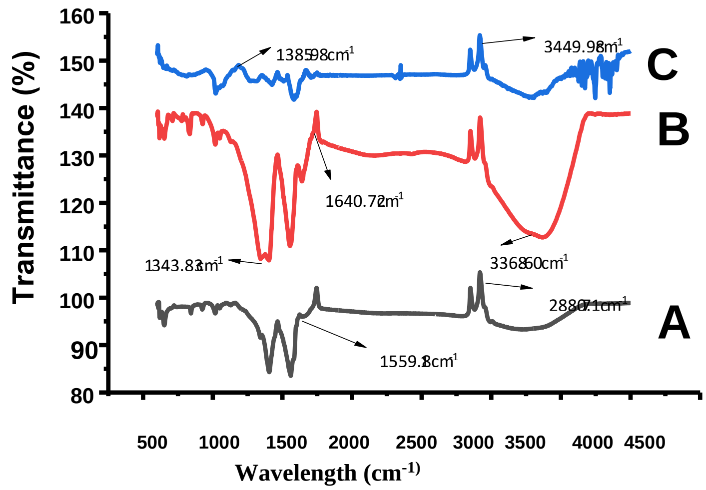

Figure 4 FT-IR data of sample as coded in the image (A) ZnO NpS and (B) Ag NO_3 NpS and (C) Ag-Zn NpS

4.1.5 SEM Analysis

Nanocomposites of Ag-Zn show that after polymerization the polymer has grown up and dispersion was better, and images show the homogeneous growth on the surfaces [11]. The average diameter of the nanocomposite was observed as 35.38nm. Figure 5 shows SEM data of the sample as coded in the image (A) ZnO NpS (B) Ag NO_3 NpS and (C) Ag-Zn NpS.

4.2 Characterization of film

4.2.1 Thickness of Film

The thickness of CS/GG, CS/GG/NLEx, CS/GG/Ag-Zn NPs, CS/GG/25NLEx/75Ag-Zn NPs, CS/GG/50NLEx/50AgZnO NPs, and CS/GG/75NLEx/25Ag-ZnNPs films is shown in Table 2. The thickness of CS/GG/Ag-Zn NPs film was observed with a lower value (0.10±0.01[c]) compared to other tested films. With a rise in polymer content, active layer thickness rose. The rise in the size of particles in the nanoparticle solution brought on by a rise in the content of polymers is what causes the active layer thickness to grow. It is noteworthy that for all particle sizes, the total thickness is 2.9±0.3 times the typical particle's radius, indicating the deposition of three layers of particles [12]. The inclusion of solid substances can have an impact on the thickness of neem leaf extract-containing films, and these solid elements can also make edible films viscous and thicker [13].

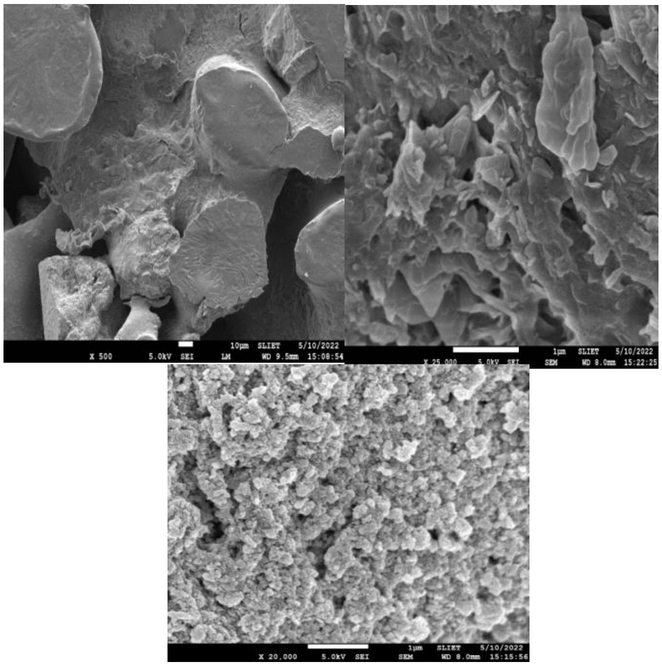

Figure 5 SEM data of sample as coded in the image (A) ZnO NpS and (B) Ag NO_3 NpS and (C) Ag-Zn NpS

4.2.2 Transparency and Opacity of Film

The transparency and opacity of films CS/GG, CS/GG/NLEx, CS/GG/Ag ZnO NPs, CS/GG/25NLEx/75Ag-Zn NPs, CS/GG/50NLEx/50Ag-Zn NPs and CS/GG/75NLEx/25AgZn NPs films are shown in Table 2. The transparency value of CS/GG/25NLEx/75Ag-Zn NPs was highest at 4.896±0.03[a] and lowest at 1.896±0.03[a] for CS/GG film. The transparency of the polymer film increased after surface alteration. At low inorganic content, the films are transparent, however, as the proportion of nanoparticles rises, they start to turn milky, indicating that light scattering plays a bigger role. The effects of adding extracts from plants on the color and transparency of the films have been examined in numerous studies [14]. Food can be safeguarded against discoloration, bad flavor, and nutrient loss by improving color properties and lowering the propensity of UV transmittance in films via plant extracts [15]. The color of the coated food product may change with higher concentrations of extracts used in the film ingredients. Additionally, opacity measures the amount of light that passes through the film surface, which is crucial for controlling light exposure to food products [16]. Also, the film's color can be a significant factor in terms of consumer perception. The opacity value of CS/GG/50NLEx/50Ag-Zn NPs was highest at 0.2989±0.05[c] and lowest at 0.0486±0.03[a] for CS/GG film.

4.2.3 Mechanical properties of film

4.2.3.1Tensile strength and elongation at break

The mechanical properties of the films are given in Table 2 The CS/GG control film showed the lowest TS value at 35.84 MPa and CS/GG/25NLEx/75Ag-Zn NPs at 47.92 MPa showed the highest TS. Adding neem leaf extract enhances the film's tensile strength, attributed to the microfibers and polyphenols present in the extract. Moreover, the tensile strength of the hybrid nanocomposite films surpassed that of the matrix and demonstrated an increase with higher concentrations [12].

The elongation at the break value of the CS/GG film was 39.56% highest among other films and the lowest value observed in CS/GG/75NLEx/25Ag-Zn NPs was 17.27%. The reduction in elongation at the break of the film upon adding extract and nanoparticles can be attributed to the interaction of chitosan with neem leaf extract and Ag-Zn NPs. This interaction enhances polymer compatibility and decreases film flexibility [13].

Table 2 Thickness, transparency, Opacity, tensile strength, and elongation of films

Film sample	Thickness (mm)	Transparency	Opacity	Tensile strength (MPa)	Elongation at break (%)
CS/GG	0.10± 0.01[b]	1.896±0.03[c]	0.0486± 0.03[c]	35.84± 0.13[c]	39.56± 0.53[a]
CS/GG/NLEx	0.13± 004[b]	2.185±0.02[b]	0.1086± 0.03[b]	40.24± 0.12[b]	27.27± 0.07[b]
CS/GG/Ag-Zn NPs	0.15± 0.02[b]	2.889±0.05[b]	0.1850± 0.02[b]	44.22± 0.25[a]	29.69± 0.05[b]
CS/GG/25NLEx/75Ag-Zn NPs	0.29± 0.02[a]	4.896±0.03[a]	0.2850± 0.02[a]	47.92± 0.75[a]	23.43± 0.65[b]
CS/GG/50NLEx/50Ag-Zn NPs	0.21± 0.02[a]	4.387±0.02[a]	0.2989± 0.05[a]	45.84± 0.18[a]	21.39± 0.15[b]
CS/GG/75NLEx/25Ag-Zn NPs	0.19± 0.02[c]	4.223±0.05[a]	0.2744± 0.05[a]	42.84± 0.23[b]	17.27± 0.07[c]

Mean ± SD values in columns followed by different letters are significantly ($p<0.05$) different. Results are means of triplicate determinations.

4.2.4 Color of film

The color value of CS/GG, CS/GG/NLEx, CS/GG/Ag-Zn NPs, CS/GG/25NLEx/75Ag-Zn NPs, CS/GG/50NLEx/50Ag-Zn NPs and CS/GG/75NLEx/25Ag-Zn NPs films is shown in Table 3. The presence of packaging film may influence the polymeric packaging material's color variables, which has an additional impact on whether consumers will accept packaged goods. The neat control films showed the maximum darkness (lowest L* value). As the concentration of extract and nanoparticles increases, there is a corresponding increase in lightness that showed that the film turned more translucent and colorless, and the higher values of a* and b*, showed that the prepared film's color was leaning towards whiteness. Table 3 showed that the phenolic constituent contained in the prepared films was most probably what caused the color shift. Chemical constituents and the number of color pigments present in polyphenolic compounds were both attributed to contributing to the phenolic constituents incorporated into films [18]. The color value of 32.26 corresponding to L* for films was higher. On the other hand, the decreased a* (-2.45, -2.56) and b* (2.43, 3.51) values of films indicate a slightly greenish-yellow color.

Table 3 Color parameters of films

Film sample	L*	a*	b*
CS/GG	31.34±0.10[a]	-2.85±0.10[b]	3.75±0.02[c]
CS/GG/NLEx	19.93±0.10[c]	-4.96±0.02[c]	12.71±0.03[a]
CS/GG/Ag-Zn NPs	32.26±0.10[a]	-2.45±0.02[b]	3.51±0.02[c]
CS/GG/25NLEx/75 Ag-Zn NPs	27.32±0.10[b]	-3.38±0.02[c]	7.47±0.02[b]
CS/GG/50NLEx/50 Ag-Zn NPs	26.13±0.10[b]	0.167±0.02[a]	9.08±0.02[b]
CS/GG/75NLEx/25 Ag-Zn NPs	32.15±0.10[a]	-2.56±0.10[b]	2.43±0.02[c]

Mean ± SD values in a column followed by different letters are significantly ($p<0.05$) different. Results are means of triplicate determinations

4.2.5 Moisture content of film

The moisture content of the film depends on the polymer used for making a film and the type of nanofiller used. Packaging films should comprise low moisture content if these are to be utilized for the packaging of food. Chitosan control film has a lower moisture content than the chitosan film containing Ag-ZnNP, due to the interaction of nanoparticles with the hydroxyl polymer group making them more hydrophilic [19]. The moisture content of the CS/GG/NLEx film was found to be lower (12.65±0.37%), whereas the highest % moisture was observed for CS/GG/50NLEx/50Ag-Zn NPs (15.65%±0.37%). These findings indicate that increasing the concentration of neem leaf extract in the matrix of chitosan-based films led to higher moisture content, likely due to molecular interactions and changes in the hygroscopic properties of the chitosan matrix. Similar observations were reported by [20].

4.2.6 Solubility in water

Water Solubility of CS/GG, CS/GG/NLEx, CS/GG/Ag-Zn NPs, CS/GG/25NLEx/75Ag-Zn NPs, CS/GG/50NLEx/50Ag-Zn NPs, and CS/GG/75NLEx/25Ag-Zn NPs films are shown in Table 4 Water solubility reflects the water resistance of film and its integrity in water. The water solubility of the film was lowest for CS/GG/25NLEx/75AgZnO NPs film at 41.32% and highest at 57.93% for CS/GG films. The incorporation of neem leaf and nanoparticles into chitosan films caused a 60% decrease in Water Solubility reported by [21]. The incorporation of extract reduced the soluble matter and subsequently the solubility. The breakdown of hydrophilic polymers occurs when water infiltrates the polymer bulk, causing swelling and eventually disrupting intermolecular forces like hydrogen bonds and Van der Waals forces between polymer chains. A slower disintegration rate indicates strong cohesion within the polymer matrix due to numerous interactions such as hydrogen bonding between polymer chains. A low percentage of water solubility designates that the film can assist or raise product integrity, hence considered a good film for water resistance [22].

4.2.7 Water vapor transmission rate (WVTR)

WVTR of CS/GG, CS/GG/NLEx, CS/GG/Ag-ZnNPs, CS/GG/25NLEx/75Ag ZnNPs, CS/GG/50NLEx/50Ag ZnNPs and CS/GG/75NLEx/25Ag-ZnNPs films were shown in Table 4. The rate at which water vapor permeates through a film under specific conditions of temperature and relative humidity is referred to as WVTR (Water Vapor Transmission Rate). This measurement is typically expressed in US standard units of g/100 in²/24 hr and metric (SI) units of g/m²/24 hr. Many polymers, particularly polar polymers, exhibit a "nonideal" behavior for the pervasion of water vapor. Owing to swelling, the water vapor permeability coefficient at polar polymers rises with higher relative humidity, which causes their sorption isotherms to deviate from Henry's law [23]. The highest WVTR value observed for the chitosan film in this study was attributed to the strong affinity of chitosan for water molecules. The WVTR values of the film samples are presented in Table 4. The CS/GG film exhibited a higher value of 4.14 (g/m²/24h) × 10^-3 compared to the CS/GG/75NLEx/25Ag-Zn NPs film, which showed a WVTR value of 3.14 (g/m²/24h) × 10^-3 ($p < 0.05$). This indicates that the addition of Ag-Zn NPs significantly reduced the WVTR value of the CS/GG/75NLEx/25Ag-Zn NPs film. Moreover, the WVP of CS/GG was high at 1.79 g m $day^{-1}p^{-1}m^{-2}10^{-10}$, and CS/GG/ 75NLEx/25Ag-Zn NPs film shows a WVTR value of 1.04 g m $day^{-1}p^{-1}m^{-2}10^{-10}$ ($p < 0.05$).

4.2.8 Antioxidant activity and total phenol content (TPC)

The TPC value of the film is highly significant due to its correlation with antioxidant activity and other physicochemical properties of the films. The highest TPC (53.86 mg GAE/g film) was observed in the film incorporating 50% silver nitrate and zinc oxide nanocomposite nanoparticles (Ag-Zn NPs) along with neem leaf extract, while the lowest TPC value (18.48 mg GAE/g) was found in the CS/GG film (Table 4). The phenolic content in the control film was attributed to the reaction between the Folin-Ciocalteu reagent and the –NH2 functional groups present in chitosan. In the blended films, phenolic content increases because of neem leaf extract and Ag-Zn NPs in the film as reported by [24]. The highest Antioxidant activity (69.92%) was observed in film incorporating 50% silver nitrate and zinc oxide nanocomposite nanoparticle (Ag-Zn NPs) and neem leaf extract and while lowest (18.52%) in CS/GG film. This activity can be attributed to the existence of the main antioxidants azadirachtin and nimbolide present in the neem leaf extract however, it could also be because of the presence of nanoparticles of silver nitrate with zinc oxide. Chitosan's antioxidant capability has been demonstrated previously, which is attributed to the presence of nitrogen at the C2 position in its polymeric structure [25].

Table 4 Moisture content, Water Solubility, Water vapor transmission rate, antioxidant activity, and total phenol content of films

Film sample	Moisture content (%)	Solubility (%)	WVTR (g /m^2/24 h)10^{-3}	WVP (g m $day^{-1}p^{-1}m^{-2}$) 10-10	Total phenol content (mg GAE/g Film)	Antioxidant activity (%)
CS/GG	12.72±0.5^{c}	57.93±0.13^{a}	4.14±0.05^{a}	1.79±0.15^{a}	18.48±0.09^{c}	18.52±0.49^{c}
CS/GG/NLEx	12.65±0.37^{c}	48.99±0.15^{b}	3.64±0.01^{b}	1.64±0.01^{a}	39.99±0.06^{b}	59.05±0.14^{b}
CS/GG/Ag-Zn NPs	14.11±0.42^{b}	50.65±0.74^{a}	3.24±0.04^{c}	1.24±0.04^{b}	45.86±0.05^{b}	69.65±0.36^{a}
CS/GG/25NLEx/75Ag-Zn NPs	14.1±0.42^{b}	41.32±0.87^{c}	3.57±0.04^{b}	1.22±0.04^{b}	49.99±0.47^{a}	65.86±0.15^{a}
CS/GG/ 50NLEx/50Ag-Zn NPs	15.65±0.37^{a}	43.76±0.43^{c}	3.18±0.05^{c}	1.38±0.05^{b}	53.86±0.07^{a}	69.92±0.07^{a}
CS/GG/ 75NLEx/25Ag-Zn NPs	15.1±0.42^{a}	47.05±0.67^{b}	3.21±0.06^{c}	1.04±0.06^{c}	47.86±0.05^{a}	63.06±0.11^{a}

4.2.9 X-ray diffraction pattern for film

The XRD analysis was performed to understand the crystal size was calculated in nanometers for different values for 2Ɵ (Figure 6). The measurement of rise in crystalline size in the range of 29.82, 32.14, and 33.24 nm, caused by grain growth, is another indication of this. A better crystalline quality is indicated by a smaller value for the crystallite size and a higher value for the dislocation density (inversely proportional). The diffraction peaks at 2θ = 31.7056, 35.5562, 38.7329, and 45.4341 observed in the cross-linked chitosan film confirm its crystalline structure in conjunction with guar gum. Similarly, sharp diffraction peaks at 2θ = 31.7086, 35.5571, 38.7235, and 45.4438 in the cross-linked composite film also affirm the crystalline structure of the guar gum film. The X-ray diffraction of nanocomposite films [26].

4.2.10 Fourier transform infrared spectroscopy (FT-IR)

Chitosan FT-IR spectra observed sharp peaks at 727.91 cm–1 (out-of-plane bending NH, out-of-plane bending C–O), 875 cm–1 (out-of-plane bending NH), 1174 cm–1 (C–O–C stretching), 142.699 cm–1 (CH2 stretching), and 3630 cm–1 (−OH stretching) (Figure 7). The vibrational mode of amide C═O stretching was observed at 875 and 108.91 cm–1 as observed by (Verma et al., 2020). The FT-IR spectra of Chitosan were also studied Stretching was detected at 3368.40 cm-1, characteristics of a carboxyl group in an aldehyde (C=O), and the presence of the stretch at 1543 cm−1, a characteristic of carboxyl-ate (COO−), indicates oxidation of the polymer over time [19].

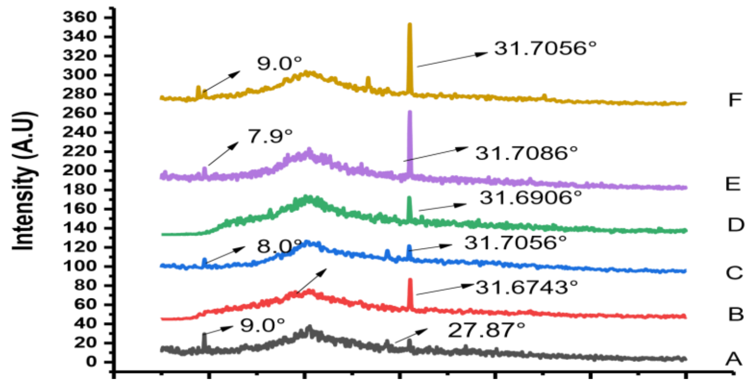

Figure 6 XRD data of sample as coded in the image A (CS/GG), B(CS/GG/NLEx), C(CS/GG/Ag-Zn NPs), D (CS/GG/25NLEx/75Ag-Zn NPs), E (CS/GG/ 50NLEx/50Ag-Zn NPs), &F (CS/GG/ 75NLEx/25Ag-Zn NPs)

After film formation, some differences were observed in the spectrum of chitosan film because of glycerol and film matrix (1% acetic acid solution). The FT-IR spectrum shows the chemical structure of protein near 698.2cm^{-1} and shows the C=O group at 1641.4cm^{-1} and 1317.04cm^{-1}. The absorption band in the range of 1300 cm^{-1} to 1450 cm^{-1} indicates the presence of flavonoids and terpenoids in neem leaf extract. The absorption band at 2334.9 cm^{-1} corresponds to the stretching vibration of the conjugated peptide bond involving amine and ketone groups [27].

There was no apparent difference in absorbance between the control film and the film being compared in the ranges of 3000 to 2900 cm^{-1} (C-H stretching vibrations) and 1500 to 1700 cm^{-1} (C=O stretching vibrations). The presence of the O-H groups, which diminished as the neem was added to the film, was attributed to the wide peak seen between 3100 and 3500 cm^{-1}. The predominant functional groups identified were -OH, C-H, C-O, and C=O. The existence of the O-H groups, which diminished as the neem was added to the film, was attributed to the wide peak seen between 3100 and 3500 cm^{-1} [28].

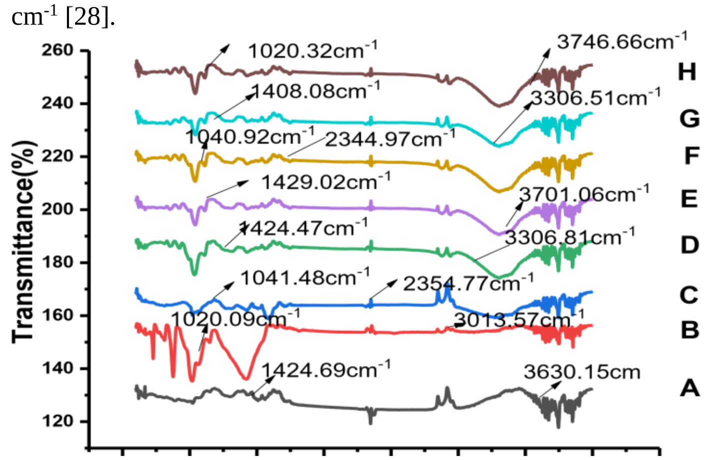

Figure 7 FT-IR data of sample as coded in the image A(CS/GG), B(CS/GG/NLEx), C(CS/GG/Ag-Zn NPs), D

(CS/GG/25NLEx/75Ag-Zn NPs), E (CS/GG/ 50NLEx/50Ag-Zn NPs),&F (CS/GG/ 75NLEx/25Ag-Zn NPs)

4.2.11 Scanning electron microscopy (SEM)

The outer surface of the control sheet was uniformly smooth and devoid of air bubbles. (Figure 8). The outer layer of the composite film displayed a more abrasive finish and more heterogeneous coat with pores after the addition of the neem leaf extracts at ratios of 25 w/w% and 75 w/w% nanoparticles into the control film. This might be an outcome of the neem leaf extract's inadequate dispersion within the chitosan guar gum polymer matrix. This was the same as reported by (Li et al., 2014) on gelatin-based films incorporated with natural antioxidants. The voids in the 50 w/w% of neem leaf extract and 50 w/w % of Ag-Zn nanoparticles films, were due to the poor dispersion and agglomeration of neem leaf extract. These results were in line with previous findings on other compound films, such as those that included carrageenan and Satureja hortensis essential oil [29].

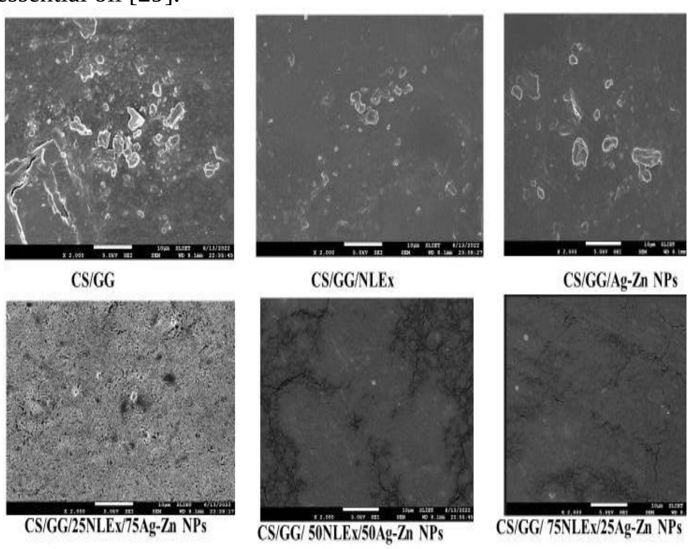

Figure 8 SEM data of sample as coded in the image A(CS/GG), B(CS/GG/NLEx), C(CS/GG/Ag-Zn NPs), D (CS/GG/25NLEx/75Ag-Zn NPs), E (CS/GG/ 50NLEx/50Ag-Zn NPs),&F (CS/GG/ 75NLEx/25Ag-Zn NPs)

4.2.12 Thermal Properties of Films

Differential scanning calorimetry (DSC) measures the energy absorbed or emitted by a sample as a function of temperature (Figure 9). The maximum point in the first control endothermic peak is related to the melting point (Tm). As it can be understood from thermograms, the addition of nanoparticles and extract of neem leaf to film formulation has changed the thermal stability of films because melting temperatures of 173.98, 261.96, 205.94, 262.20, and 242.90°C are related to films containing 25:75, 50:50 and 75:25 neem leaf extract and Ag-Zn NPs respectively. Higher concentrations of chitosan can enhance hydrogen bonding, thereby increasing viscosity and activation energy for diffusion, potentially leading to a lower melting point with increased concentrations of extract and nanoparticles. This phenomenon could restrict the mobility of polymer chains, thereby reducing crystal growth and nucleation [30].

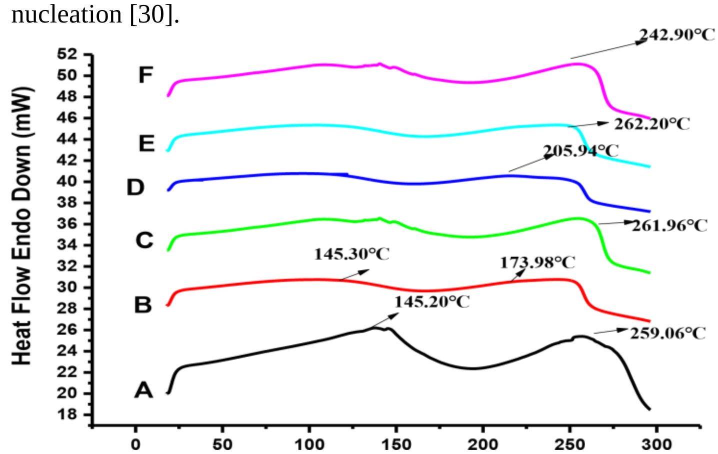

Figure 9 DSC data of sample as coded in the image A(CS/GG), B(CS/GG/NLEx), C(CS/GG/Ag-Zn NPs), D (CS/GG/25NLEx/75Ag-Zn NPs), E (CS/GG/ 50NLEx/50Ag-ZnNPs),&F (CS/GG/ 75NLEx/25Ag-Zn NPs)

5. Conclusion

In the present work, a technique for the synthesis of Ag-Zn stabilized with chitosan and guar gum was developed. Ag-Zn NPs with green combustion method based on neem leaf extract. It is an environmentally friendly, straightforward, and cost-effective method for synthesizing nanoparticles. Moreover, nanocomposites of silver nitrate and zinc oxide have better antioxidant property, more crystalline. The optimized CS/GG/50NLEx/50Ag-Zn NPs overall have better mechanical, thermal, optical, and antioxidant or phenolic properties. The resulting film was transparent, homogeneous, and had good barrier properties. This study introduced a novel method for producing chitin, guar gum, glycerol, and neem leaf extract-based composite films, which hold promise for diverse applications, particularly in packaging

References

[1] Braga, T. M., Rocha, L., Chung, T. Y., Oliveira, R. F., Pinho, C., Oliveira, A. I., ... & Cruz, A. (2020). Biological activities of gedunin—a limonoid from the meliaceae family. Molecules, 25(3), 493.

[2] Silva, S., Almeida, A. J., & Vale, N. (2021). Importance of nanoparticles for the delivery of antiparkinsonian drugs. Pharmaceutics, 13(4), 508.

[3] Dash, K. K., Deka, P., Bangar, S. P., Chaudhary, V., Trif, M., & Rusu, A. (2022). Applications of inorganic nanoparticles in food packaging: a comprehensive review. Polymers, 14(3), 521.

[4] Gordienko, M. G., Palchikova, V. V., Kalenov, S. V., Belov, A. A., Lyasnikova, V. N., Poberezhniy, D. Y., & Skladnev, D. A. (2019). Antimicrobial activity of silver salt and silver nanoparticles in different forms against microorganisms of different taxonomic groups. Journal of Hazardous Materials, 378, 120754

[5] Liu, Q., Li, J., Zhong, X., Dai, Z., Lu, Z., Yang, H., & Chen, R. (2018). Enhanced antibacterial activity and mechanism studies of ag/bi2o3 nanocomposites. Advanced powder technology, 29(9), 2082-2090.

[6] Voss, G. T., Gularte, M. S., Vogt, A. G., Giongo, J. L., Vaucher, R. A., Echenique, J. V., ... & Fajardo, A. R. (2018). Polysaccharide-based film loaded with vitamin c and propolis: a promising device to accelerate diabetic wound healing. International Journal of Pharmaceutics, 552(1-2), 340-351

[7] Slathia, S., Gupta, T., & Chauhan, R. P. (2021). Green synthesis of Ag–ZnO nanocomposite using azadirachta indica leaf extract exhibiting excellent optical and electrical properties. Physica b: condensed matter, 621, 413287.

[8] Yadav, M., Behera, K., Chang, Y. H., & Chiu, F. C. (2020). Cellulose nanocrystal reinforced chitosan based uv barrier composite films for sustainable packaging. Polymers, 12(1), 202.

[9] Zare, M., Namratha, K., Byrappa, K., Surendra, D. M., Yallappa, S., & Hungund, B. (2018). Surfactant assisted solvothermal synthesis of zno nanoparticles and study of their antimicrobial and antioxidant properties. Journal of Materials Science & Technology, 34(6), 1035-1043

[10] Ates, M., & Topkaya, E. (2015). Nanocomposite film formations of polyaniline via TiO2, Ag, and Zn, and their corrosion protection properties. *Progress in Organic Coatings*, *82*, 33-40.

[11] Krishnamurthy, A., & Amritkumar, P. (2019). Synthesis and characterization of eco-friendly bioplastic from low-cost plant resources. Sn applied sciences, 1(11), 1-13.

[12] Ulum, M. S., Sesa, E., & Belcher, W. (2021). The effect of polymer concentration in chloroform on p3ht: pcbm nanoparticulate organic photovoltaic device performance. In journal of physics: conference series (vol. 1763, no. 1, p. 012073). Iop publishing.

[13] Munir, S., Javed, M., Hu, Y., Liu, Y., & Xiong, S. (2020). The effect of acidic and alkaline ph on the physico-mechanical properties of surimi-based edible films incorporated with green tea extract. Polymers, 12(10), 2281

[14] Moraczewski, K., Pawłowska, A., Stepczyńska, M., Malinowski, R., Kaczor, D., Budner, B., ... & Rytlewski, P. (2020). Plant extracts as natural additives for environmentally friendly polylactide films. Food packaging and shelf life, 26, 100593.

[15] Arfat, Y. A., Ahmed, J., Hiremath, N., Auras, R., & Joseph, A. (2017). Thermo-mechanical, rheological, structural and antimicrobial properties of bionanocomposite films based on fish skin gelatin and silver-copper nanoparticles. Food hydrocolloids, 62, 191-202.

[16] Ma, W., Rokayya, S., Xu, L., Sui, X., Jiang, L., & Li, Y. (2018). Physical-chemical properties of edible film made from soybean residue and citric acid. Journal of Chemistry, 2018.

[17] Kalia, A., Kaur, M., Shami, A., Jawandha, S. K., Alghuthaymi, M. A., Thakur, A., & AbdElsalam, K. A. (2021). Nettle-leaf extract derived zno/cuo nanoparticle-biopolymer-based antioxidant and antimicrobial nanocomposite packaging films and their impact on extending the post-harvest shelf life of guava fruit. Biomolecules, 11(2), 224.

[18] Singh, T., Saini, H. S., Ranganayakulu, S. V., Ravi, S., & Sudhakar, K. (2017). Molecular docking assisted isolation of azadirachtin-a., from seeds of *Azadirachta indica* extract against cervical cancer. Ind. J. Sci. Technol, 10.

[19] Kalia, A., Kaur, M., Shami, A., Jawandha, S. K., Alghuthaymi, M. A., Thakur, A., & AbdElsalam, K. A. (2021). Nettle-leaf extract derived zno/cuo nanoparticle-biopolymer-based antioxidant and antimicrobial nanocomposite packaging films and their impact on extending the post-harvest shelf life of guava fruit. Biomolecules, 11(2), 224.

[20] Kumar, N. (2019). Polysaccharide-based component and their relevance in edible film/coating: a review. Nutrition & Food Science.

[21] Santos, F. K. G. D., Silva, K. N. D. O., Xavier, T. D. N., Leite, R. H. D. L., & Aroucha, E. M. M. (2017). Effect of the addition of carnauba wax on physicochemical properties of chitosan films. Materials Research, 20, 479-484.

[22] Binti Che Wan, N. H., Nafchi, A. M., & Huda, N. (2018). Film opacity, water vapor permeability, water solubility and fourier transform infrared radiation (ftir) of a biodegradable film based on a duck feet gelatin and polyvinyl alcohol blend. Asia Pacific Journal of Sustainable Agriculture, Food and Energy, 6(2), 10-15.

[23] Turan, D. (2021). Water vapor transport properties of polyurethane films for packaging of respiring foods. Food engineering reviews, 13(1), 54-65.

[24] Bajić, M., Novak, U., & Likozar, B. (2019, January). Development of bio-based chitosan films with incorporated chestnut extract. In proceedings of the world congress on mechanical, chemical, and material engineering. Avestia publishing.

[25] Aziz, S. B., Karim, W. O., Brza, M. A., Abdulwahid, R. T., Saeed, S. R., Al-Zangana, S., & Kadir, M. F. Z. (2019). Ion transport study in CS: POZ based polymer membrane electrolytes using Trukhan model. *International journal of molecular sciences*, *20*(21), 5265.

[26] Pinheiro, C. P., Mello, T. G., Vieira, M. L., & Pinto, L. A. (2019). Chitosan-coated different particles in spouted bed and their use in dye continuous adsorption system. *Environmental Science and Pollution Research*, *26*(28), 28510-28523.

[27] Kumar, U. S. U., Paridah, M. T., Owolabi, F. T., Gopakumar, D. A., Rizal, S., Amirul, A. A., ... & Khalil, H. A. (2019). Neem leaves extract based seaweed bio-degradable composite films with excellent antimicrobial activity for sustainable packaging material. Bioresources, 14(1), 700-713.

[28] Oyekanmi, A. A., Kumar, U., Hps, A. K., Olaiya, N. G., Amirul, A. A., Rahman, A. A., ... & Rizal, S. (2021). Functional properties of antimicrobial neem leaves extract based macroalgae biofilms for potential use as active dry packaging applications. Polymers, 13(10), 1664.

[29] Vu, H. P. N., & Lumdubwong, N. (2016). Starch behaviors and mechanical properties of starch blend films with different plasticizers. Carbohydrate polymers, 154, 112-120.

[30] Rubilar, J. F., Cruz, R. M., Silva, H. D., Vicente, A. A., Khmelinskii, I., & Vieira, M. C. (2013). Physico-mechanical properties of chitosan films with carvacrol and grape seed extract. Journal of Food Engineering, 115(4), 466-474.